LETTER

doi:10.1038/nature10528

Laser cooling and real-time measurement of the nuclear spin environment of a solid-state qubit

E. Togan[1]*, Y. Chu[1]*, A. Imamoglu[2] & M. D. Lukin[1]

Control over quantum dynamics of open systems is one of the central challenges in quantum science and engineering. Coherent optical techniques, such as coherent population trapping involving dark resonances[1,2], are widely used to control quantum states of isolated atoms and ions. In conjunction with spontaneous emission, they allow for laser cooling of atomic motion[3], preparation and manipulation of atomic states[4], and rapid quantum optical measurements that are essential for applications in metrology[5–7]. Here we show that these techniques can be applied to monitor and control individual atom-like impurities, and their local environment[8–11], in the solid state. Using all-optical manipulation of the electronic spin of an individual nitrogen–vacancy colour centre in diamond, we demonstrate optical cooling, real-time measurement and conditional preparation of its nuclear spin environment by post-selection. These methods offer potential applications ranging from all-optical nanomagnetometry to quantum feedback control of solid-state qubits, and may lead to new approaches for quantum information storage and processing

Over the past two decades, coherent population trapping (CPT) has been used in the laser cooling of neutral atoms and ions[3], the creation of ultracold molecules[4], optical magnetometry[5,6], and atomic clocks[7], as well as in slowing and stopping light pulses[2]. The electronic spin of the nitrogen–vacancy (NV) centre is a promising system for extending these techniques to the solid state. The NV centre has a long-lived spin triplet as its electronic ground state[12], whose $m_S = \pm 1$ and $m_S = 0$ sublevels we denote by $|\pm 1\rangle$ and $|0\rangle$. In pure samples, the electron spin dynamics are governed by interactions with the spin-1 ^{14}N nucleus of the NV centre and spin-1/2 ^{13}C nuclei present in 1.1% natural abundance in the diamond lattice (Fig. 1a). Control over nuclear spins[13,14] is of interest both for fundamental studies and in applications such as nanoscale magnetic sensing[15,16] and the realization of quantum networks[17,18]. Here we achieve such control by two complimentary methods: effective cooling of nuclear spins through nuclear-state-selective CPT[8], and conditional preparation based on fast measurements of the nuclear environment and subsequent post-selection[11].

Whereas most previous work involved the use of microwave and radio-frequency fields to manipulate both the electronic and the nuclear spin states, we use all-optical control of the electronic spin[19–21]. Specifically, we make use of Λ-type level configurations involving the NV centre's optically excited electronic states $|A_1\rangle$ and $|A_2\rangle$ and the

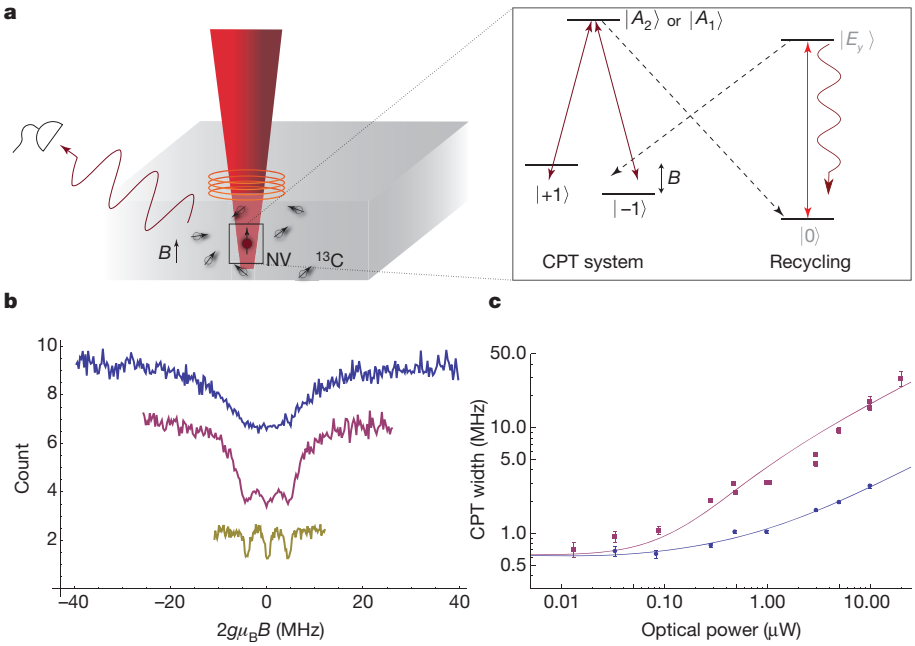

Figure 1 | Coherent population trapping in NV centres. **a**, The Λ-type transitions between the ground states $|\pm 1\rangle$ and excited states $|A_1\rangle$ and $|A_2\rangle$ of a single NV centre are addressed with a CPT laser, while a recycling laser drives the $|0\rangle \rightarrow |E_y\rangle$ transition. An external magnetic field, B, is applied using a solenoid. **b**, Photon count from NV centre NVa in a 300-μs window are plotted versus the applied field for three different powers of a laser addressing the state $|A_2\rangle$: blue, 10 μW; pink, 3 μW; yellow, 0.1 μW. The blue and pink data sets are shifted vertically by five and, respectively, two counts for clarity. μ_B, Bohr magneton; g, gyromagnetic ratio. **c**, Width of individual ^{14}N CPT lines versus CPT laser power when the $|A_1\rangle$ (blue) or $|A_2\rangle$ (pink) state is used. Solid curves represent the theoretical model discussed in the main text and Supplementary Information. Error bars, s.d.

[1]Department of Physics, Harvard University, Cambridge, Massachusetts 02138, USA. [2]Institute for Quantum Electronics, ETH-Zurich, CH-8093 Zurich, Switzerland.
*These authors contributed equally to this work.

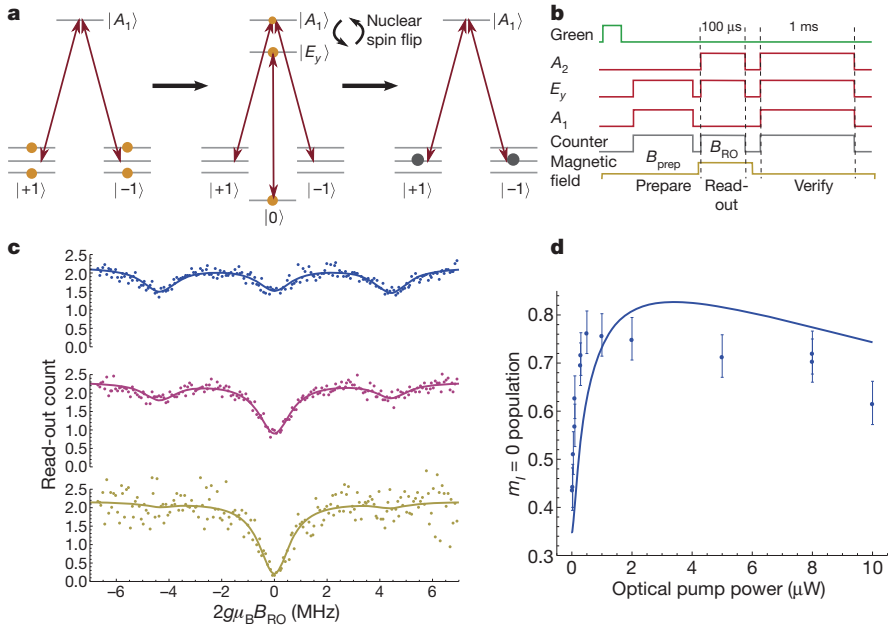

Figure 2 | Optical control and conditional preparation of the proximal ^{14}N nuclear spin. **a**, Mechanism for optical pumping of ^{14}N states. **b**, Pulse sequence for ^{14}N optical pumping using the laser addressing the state $|A_1\rangle$ (A_1 laser) and a fixed read-out of the prepared state using the A_2 laser. To ensure that the nitrogen–vacancy was not ionized for all subsequent data runs, we turn on all three lasers at the end of each run so that there is no dark state, and only keep data from runs in which we obtain a high number of counts during this verification step. **c**, Counts collected with NVa during the read-out step versus the read-out magnetic field when there is no preparation step (blue) and when there is preparation with optical pumping using 100 nW of A_1 laser power for 1.9 ms (pink). The yellow curve shows the results of ^{14}N polarization through measurement-based preparation by selecting the read-out events in which the number of counts collected during the last 500 µs of preparation is zero (Supplementary Information, section 4.2). **d**, Steady-state population in the $m_I = 0$ state after optical pumping for varying powers of the A_1 laser, with theoretical model described in Supplementary Information (solid line). Error bars, s.d.

$|\pm1\rangle$ ground states[18,22] (Fig. 1a). At low temperatures (<10 K) and in the limit of zero strain, $|A_1\rangle$ and $|A_2\rangle$ are entangled states of spin and orbital momentum, both coupled to $|+1\rangle$ with σ_--polarized light and to $|-1\rangle$ with σ_+-polarized light. Correspondingly, excitation with linearly polarized light drives the NV centre into a 'dark' superposition state when the two-photon detuning is zero[1]. In the present case, the two-photon detuning is determined by the Zeeman splitting between the $|\pm1\rangle$ states due to the combined effect of the Overhauser field originating in the nuclear spin environment and any externally applied magnetic field[8,10]. When the external field exactly compensates the Overhauser field, the electronic spin of the NV centre is pumped into the dark state after a few optical cycles and remains in there, resulting in vanishing fluorescence. This is the basis of the dark resonances and CPT.

In our experiments, $|A_1\rangle$ and $|A_2\rangle$ are separated in energy by an amount corresponding to ~3 GHz and are addressed individually with a single, linearly polarized laser at near-zero magnetic field. Because there is a finite branching ratio from the $m_S = \pm1$ manifold of the electronic spin into state $|0\rangle$, we use a recycling laser that drives the transition between $|0\rangle$ and the excited state $|E_y\rangle$, which decays with a small but non-vanishing probability (~10^{-2}) back to the states $|\pm1\rangle$. In Fig. 1b, we present our observations of the CPT spectrum as a function of an external magnetic field at three different powers of a laser tuned to the $|\pm1\rangle \rightarrow |A_2\rangle$ transition. A broad resonance is observed at high powers, but as the power is reduced we clearly resolve three features in the spectrum, separated by 4.4 MHz, which is twice the hyperfine splitting between three ^{14}N nuclear spin states. This separation corresponds to the magnetic field required to bring the electronic $m_S = \pm1$ hyperfine states with equal nuclear spin projections ($m_I = \pm1, 0$) into two-photon resonance.

The dependence of the CPT resonance width on the laser power (Fig. 1c) shows that repumping on the transition $|0\rangle \leftrightarrow |E_y\rangle$ has an important role in our experiment. By contrast with a conventional, closed three-level system, this recycling transition can be used to enhance the utility of our CPT system by both decreasing the width of the CPT resonance and increasing the signal-to-noise ratio. The state $|A_1\rangle$ decays into the $m_S = 0$ ground state through the NV centre's metastable singlet state with a substantial probability, of ~40% (Supplementary Information). However, the population returns to the $m_S = \pm1$ state from $|E_y\rangle$ after only ~100 optical excitation cycles. As a result, away from the two-photon resonance, the NV centre quickly decays to $|0\rangle$ after being excited, and then scatters many photons through the transition $|0\rangle \leftrightarrow |E_y\rangle$ before returning to the Λ system (the Λ-type level configuration described above). If the NV centre is not in a dark state, this process effectively increases the number of photons we collect by a factor of $2/\eta = \gamma_{s1}/\gamma_{ce}$, where γ_{ce} is the cross-transition rate from $|E_y\rangle$ into $|\pm1\rangle$ and γ_{s1} is the transition rate from $|A_1\rangle$ to the singlet. The cycling effect also reduces the width of the CPT line because the $|0\rangle \leftrightarrow |E_y\rangle$ transition quickly saturates away from two-photon resonance, provided that the CPT laser excitation rate exceeds the rate of leakage out of the recycling transition. Significantly, both of these effects lead to improved sensitivity of dark resonances to small changes in two-photon detuning.

To demonstrate this increase in sensitivity, in Fig. 1c we compare the widths of dark resonances observed through excitation of $|A_1\rangle$ and $|A_2\rangle$. Through independent measurements of the branching ratios (Supplementary Information), we determined that $|A_1\rangle$ and $|A_2\rangle$ correspond to an open and, respectively, nearly closed Λ systems, with $\eta_{A_1} \approx 3.1 \times 10^{-2}$ and $\eta_{A_2} \approx 2.6$. We compare these experimental results with a theoretical model described in Supplementary Information, which predicts that the resonance linewidth, δ_0, is given by

$$\delta_0 = \sqrt{\frac{R_A^2}{1+(1/\eta)(R_A/R_E+2R_A/\gamma)}}$$
$$\approx \sqrt{R_A R_E \eta\gamma/(R_E+\gamma)}$$

for small η, where R_A and R_E correspond to the optical excitation rates of a laser tuned to states $|A_1\rangle$ or $|A_2\rangle$ and, respectively, $|E_y\rangle$, and γ is the decay rate of excited states. The width at low powers is determined by the random magnetic field associated with surrounding ^{13}C nuclear states. When this line broadening mechanism is taken into account (Supplementary Information), the experimental results are in excellent agreement with these predictions, which we plot as solid lines in Fig. 1c.

Having resolved the hyperfine coupling between the nitrogen–vacancy electron spin and ^{14}N spin, we now demonstrate optical cooling of the nuclear spin states using dark resonances. This method (Fig. 2a) is reminiscent of laser cooling of atomic motion by velocity-selective CPT[3,8]. A redistribution of the ^{14}N spin state population on optical excitation takes place because the hyperfine coupling in the excited electronic state of the NV centre is enhanced by a factor of ~20 relative to that in the ground state[23]. If the external field is set such that, for example, the $m_I = 0$ hyperfine states are in two-photon resonance, only the states with nuclear configuration $m_I = \pm 1$ will be promoted to the excited states, where flip-flops with the electron spin will change the nuclear spin state to $m_I = 0$. When the NV centre spontaneously decays into the dark superposition of electronic spin states, optical excitation will cease, resulting in effective polarization (cooling) of nuclear spin into the $m_I = 0$ state.

In Fig. 2c, we present our observations of laser cooling of ^{14}N nuclear spins by CPT. For each point, the pulse sequence shown in Fig. 2b is applied, where the magnetic field B_{prep} is kept at zero during the preparation/optical pumping process, and fluorescence is collected when the field is switched to a particular read-out value, B_{RO}. The increased contrast of the $m_I = 0$ CPT line relative to the other two corresponds to a nuclear spin polarization of 61.5 ± 4.4%. As shown in Fig. 2d, by optimizing the power of the laser tuned to $|A_1\rangle$ we achieve a maximum nuclear polarization of 76.4 ± 4.4% over a timescale of 353 ± 34 μs. The degree of polarization is probably limited by the escape rate out of the dark state due to off-resonance excitation of $|A_2\rangle$ and dephasing caused by surrounding ^{13}C nuclei. A simple theoretical model taking into account these two processes and using independently measured parameters (Fig. 2d, solid line) reproduces the qualitative features of our experimental results.

We can further improve the preparation of ^{14}N nuclear spins in a desired state by measurement and post-selection, as predicted by theoretical proposals[10,11,24]. Specifically, the observation of zero photodetection events during the preparation step at $B_{\mathrm{prep}} = 0$ determines the ^{14}N spins to be in the $m_I = 0$ state. For instances in which such a measurement result was obtained, the bottom plot of Fig. 2c shows the nuclear spin populations measured during the subsequent probe step. The resulting ^{14}N polarization, of more than 92 ± 6%, demonstrates that high-fidelity conditional preparation of nuclear spins is possible.

We next extend our technique to monitor and cool the many-body environment of the NV centre, which consists of ^{13}C nuclei distributed throughout the diamond lattice. The large number of nuclear spin configurations associated with an unpolarized environment results in a random Overhauser field, B_{Ov}, with unresolved hyperfine lines. This produces a finite CPT linewidth in measurements that average over all configurations of the ^{13}C spin bath (Fig. 1b, c). We can overcome this limitation by making fast measurements. The key idea of our approach is to use the long correlation time, T_1^{nuc}, associated with evolution of the nuclear bath, to observe its instantaneous state and its dynamics. Such a fast measurement is illustrated in Fig. 3a, where the externally applied field is ramped across a single ^{14}N $m_I = 0$ line while the CPT lasers are on. The yellow points in Fig. 3c shows the line shape averaged over many experimental runs, and the intensity plot in Fig. 3b shows counts collected in 80-μs time bins during successive individual runs, many of which distinctly show a narrow dark region. Lorentzian fits to selected experimental scans (Fig. 3c, blue and pink curves) reveal 'instantaneous' CPT resonances with linewidths that are more than a factor three less than those of the averaged measurement.

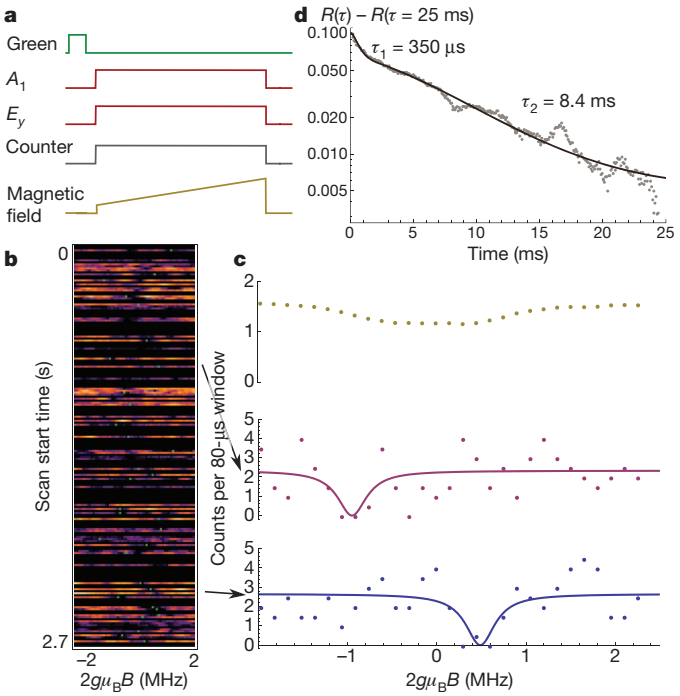

Figure 3 | Observation of instantaneous Overhauser field from the ^{13}C spin bath. **a**, Pulse sequence for real-time measurement of the ^{13}C nuclear configuration. The applied magnetic field is ramped over a single ^{14}N CPT line over 5 ms while counts are collected in 80-μs bins. **b**, Counts from 200 successive runs are shown on horizontal lines for NVb. Runs in which the verification step fails are blacked out. The centres of constrained Lorentzian fits (Supplementary Information, section 7) to individual runs are indicated with green dots. **c**, Two such individual runs are shown with their fits (pink and blue), along with an average of scans that passed verification (yellow). **d**, Autocorrelation, $R(\tau)$, of counts with magnetic field fixed at the $m_I = 1$ ^{14}N line. The fit is to a bi-exponential decay.

The change in the centres of the dark regions (Fig. 3b, green dots) indicates that the instantaneous field evolves in time.

To provide more quantitative insight into the dynamics of the nuclear environment, we record the fluorescence counts at a fixed value of the external magnetic field with a time resolution of 80 μs during 50-ms time intervals. The autocorrelation of the resulting photon detection events (Fig. 3d) reveals two distinct timescales: $\tau_1 = 350 \pm 30$ μs, consistent with the ^{14}N nuclear spin polarization timescale, and $\tau_2 = 8.40 \pm 0.20$ ms. Most notably, because we can detect dark states of the NV centre with a resolution of 80 μs, these results indicate that reliable measurement of the Overhauser field is possible within its correlation time.

We now demonstrate how fast measurements can be used to prepare conditionally the ^{13}C environment of the NV centre in a desired state with post-selection. We record counts accumulated during both the preparation step and the read-out step with relatively low power using the sequence shown in Fig. 4a. Similar to measurement-based preparation of the ^{14}N spin, by conditionally selecting zero-photon-detection events during the preparation step, we can select the states of the ^{13}C environment that have vanishing two-photon detuning ($\delta = 2g\mu_B(B_{\mathrm{prep}} + B_{\mathrm{Ov}}) = 0$). The pink curve in Fig. 4b shows (unconditioned) read-out counts recorded following the preparation step, whereas the blue curve shows the results of (conditioned) measurement-based preparation. The measured width of such a conditionally prepared distribution is significantly smaller than the width corresponding to individual ^{14}N resonances obtained without preparation. We find that although this width depends on B_{prep}, so too does the position of the narrow feature, indicating that we can conditionally prepare the ^{13}C environment by post-selection with a

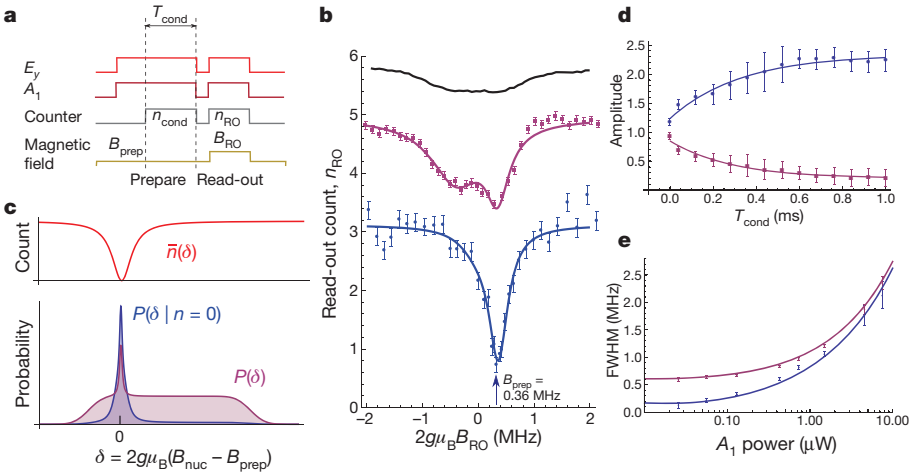

Figure 4 | Measurement-based preparation of ^{13}C spin bath. **a**, Pulse sequence for preparation and subsequent measurement of the ^{13}C configuration. B_{prep} is set within the central ^{14}N line and B_{RO} is varied to cover all associated ^{13}C states. A green laser pulse and a ^{14}N optical pumping step with the A_2 and E_y lasers (not shown) occur before this. Counts during a conditioning window of length T_{cond} (n_{cond}) at the end of preparation and during the 500-μs read-out window (n_{RO}) are recorded for each run. The data presented are an average of many such experimental runs. **b**, n_{RO} for NVb versus B_{RO} is shown in pink with double-Lorentzian fit. The same data set analysed by keeping only events with $n_{cond} = 0$ is shown in blue. The unprepared ^{13}C distribution (the same as yellow curve in Fig. 3c) is shown in black for qualitative comparison (shifted by 4.3 counts for clarity). **c**, Physics of conditional preparation through measurement. **d**, Amplitudes of broad (blue) and narrow (pink) distributions versus T_{cond} for NVb. The same data set was used for each point and the length of the conditioning window was changed in post-processing. **e**, Full-width at half-maximum (FWHM) of measured ^{13}C distribution with (blue) and without (pink) conditional preparation, versus A_1 laser power for NVa. Solid lines are theoretical predictions for the read-out linewidth, δ_0 (blue), and the CPT linewidth for the unprepared ^{13}C distribution (pink; same as in Fig. 1c). Error bars, s.d.

Overhauser field of our choice (Supplementary Fig. 8). The prepared configurations are long lived both when unilluminated ($\gg$6 ms; Supplementary Fig. 9) and in the presence of laser light, consistent with autocorrelation measurements ($\tau_2 = 8.4$ ms; Fig. 3d).

We now discuss our experimental results and explore the limits of our ability to probe and prepare the ^{13}C environment. As discussed in Methods Summary and illustrated in Fig. 4c, conditional measurement prepares an Overhauser field distribution that consists of the broad unconditioned distribution suppressed by $\exp(-CT_{cond})$ and a narrow peak with a width $\delta_c = \sqrt{\ln(2)}\delta_0/\sqrt{CT_{cond}}$, where C is the fluorescence rate of the bright state and T_{cond} is the measurement time. The read-out step itself has a 'resolution' determined by the dark-resonance linewidth, δ_0. The observed features represent a convolution of the dark-resonance probe with the conditionally prepared distribution. For the conditional preparation to be effective, we require that $CT_{cond} > 1$ and, therefore, $\delta_c < \delta_0$, indicating that the measured CPT linewidth will be limited by the read-out step. Experimentally, we find that our measured line shapes can be well fitted by a combination of two Lorentzian distributions, one narrow and one broad, whose widths and positions are only weakly dependent on photodetection time, T_{cond}. However, as T_{cond} is increased, the relative weight of the narrow distribution increases (Fig. 4d). This is consistent with the theoretical prediction that the read-out-limited width of the narrow resonance does not depend on T_{cond}, and better discrimination in conditional measurements increases the probability that the nuclear spin state is prepared in the narrow distribution.

Notably, we find that even without conditioning (Fig. 4b, pink line), a narrow distribution of nuclear spin configurations around B_{prep} is prepared. This modification of the nuclear distribution is a result of CPT-based laser cooling of the ^{13}C bath, consistent with the predictions of ref. 8. The specific physical mechanism of such cooling probably involves electronic-spin-dependent evolution of the ^{13}C nuclei, and will be discussed in detail in future studies. We emphasize that this observation provides a clear indication that the magnetic environment is affected by the dynamics of the NV centre, providing direct evidence that the nitrogen–vacancy spin dynamics is dominated by the Overhauser field rather than external magnetic field fluctuations.

Figure 4e shows how the observed linewidth of the narrow feature depends on the CPT laser power. At low powers, the observed width reaches a minimum value of 104 ± 49 kHz. This limiting width results from the effects of strain splitting of states $|\pm 1\rangle$ on the read-out process at zero magnetic field[25] (see Supplementary Information for a quantitative discussion of effects of strain). Owing to this splitting, very small magnetic field changes do not shift the energies of states $|\pm 1\rangle$ to first order. Therefore, our CPT read-out signal becomes insensitive to Zeeman shifts of the order of twice the strain splitting (Supplementary Information). In addition, a minimal linewidth of ~400 kHz was obtained for measurements performed with a separate NV centre (NVb) subject to higher strain.

The limit associated with strain splitting can be easily circumvented by using a large external magnetic field to split the spin states $|\pm 1\rangle$ and two laser frequencies to address the NV centre in a Raman configuration near zero two-photon detuning. As described in Supplementary Information, a modest increase in collection efficiency by, say, one order of magnitude[26] would allow us to obtain quantum-limited narrowing of the nuclear distribution to $\delta_c \approx 1/T_{cond}$, which, in turn, could be on the order of the inverse lifetime of the given nuclear configuration[8].

The experiments reported here offer the intriguing prospect of using coherent optical techniques to control nuclear spins surrounding quantum emitters. For instance, the technique that we describe can be used to study the quantum many-body dynamics of 'central-spin' models in real time, either in isolation or in the presence of dissipation[27]. Specific examples of this include nuclear field diffusion that, in the presence of CPT lasers, is expected to have statistical properties reminiscent of Lévy flights in velocity-selective CPT[28]. Furthermore, our approach allows for direct application of quantum feedback control to drive nuclear spins deterministically into a desired state. This may be used to prepare non-classical superposition states of nuclear spins analogous to spin-squeezed states in atomic ensembles[29], and to 'engineer' collective dissipation in nuclear spin ensembles useful for applications in quantum information science, such as the long-term storage of quantum states[30]. Finally, our method allows for an all-optical approach to magnetic sensing[5,6] that may have interesting applications in nanoscience[15,16].

METHODS SUMMARY

Sample description. The diamond sample used was a natural, high-purity, type-IIa diamond with a (111) cut, kept at ~7 K. The data presented in the main text and the Supplementary Information came from measurements on three separate NV centres in this sample. The first NV centre (NVa) was under relatively low strain and had a narrow distribution of ^{13}C states. The second, higher-strain NV centre (NVb) had a broader distribution of ^{13}C states. All experiments on optical cooling and conditional preparation were repeated using both of these NV centres, with consistent results. Figures 1, 2 and 4e and Supplementary Fig. 3 present measurements on NVa. The remaining figures in the main text and Supplementary Information, excluding Supplementary Fig. 5, present measurements on NVb. The third NV centre (NVc) was used for electron spin resonance measurements (Supplementary Information, section 5), with which we calibrated the ground-state strain for NVa and NVb by assuming that it is proportional to the strain measured using the excited states $|E_x\rangle$ and $|E_y\rangle$ (ref. 25).

Measurement-based preparation of ^{13}C environment. We consider the situation in which the NV centre is continuously monitored for a time T_{cond}. The average number of photons detected during preparation is given by $\bar{n}(\delta)T_{\mathrm{cond}}$, where the photon detection rate, $\bar{n}(\delta) = C\delta^2/(\delta_0^2+\delta^2)$, is related to the instantaneous value of the Overhauser field through the two-photon detuning, δ (Fig. 4c). Directly after preparation, the nuclear state probability distribution determined by conditioning on obtaining zero counts is $P(\delta \mid n=0)$, which is related to the conditional probability of a zero-count event, $P(n=0 \mid \delta)$, by $P(\delta \mid n=0) = P(n=0 \mid \delta)P(\delta)/P(n=0)$, where $P(n)$ and $P(\delta)$ are respectively the unconditional count and detuning distributions. For a Poisson-distributed random process of photon counts, we find that $P(\delta \mid n=0) \approx \exp\left(-CT_{\mathrm{cond}}\delta^2/\left(\delta_0^2+\delta^2\right)\right)P(\delta)$. As T_{cond} increases, the range of δ for which we obtain zero counts owing to the existence of a dark state becomes small, and, for large δ, we expect the average number of counts to be high and the probability of detecting $n=0$ counts due to shot noise to be small. This effectively reduces the width of the conditionally prepared nuclear spin distribution.

Received 13 June; accepted 31 August 2011.

1. Scully, M. O. & Zubairy, M. S. *Quantum Optics* 222–225 (Cambridge Univ. Press, 1997).
2. Fleischhauer, M., Imamoglu, A. & Marangos, J. P. Electromagnetically induced transparency: optics in coherent media. *Rev. Mod. Phys.* **77,** 633–673 (2005).
3. Aspect, A., Arimondo, E., Kaiser, R., Vansteenkiste, N. & Cohen-Tannoudji, C. Laser cooling below the one-photon recoil energy by velocity-selective coherent population trapping. *Phys. Rev. Lett.* **61,** 826–829 (1988).
4. Ni, K.-K. *et al.* A high phase-space-density gas of polar molecules. *Science* **322,** 231–235 (2008).
5. Scully, M. O. & Fleischhauer, M. High-sensitivity magnetometer based on index-enhanced media. *Phys. Rev. Lett.* **69,** 1360–1363 (1992).
6. Budker, D. & Romalis, M. Optical magnetometry. *Nature Phys.* **3,** 227–234 (2007).
7. Vanier, J. Atomic clocks based on coherent population trapping: a review. *Appl. Phys. B* **81,** 421–442 (2005).
8. Issler, M. *et al.* Nuclear spin cooling using Overhauser-field selective coherent population trapping. *Phys. Rev. Lett.* **105,** 267202 (2010).
9. Xu, X. *et al.* Optically controlled locking of the nuclear field via coherent dark-state spectroscopy. *Nature* **459,** 1105–1109 (2009).
10. Stepanenko, D., Burkard, G., Giedke, G. & Imamoglu, A. Enhancement of electron spin coherence by optical preparation of nuclear spins. *Phys. Rev. Lett.* **96,** 136401 (2006).
11. Giedke, G., Taylor, J. M., D'Alessandro, D., Lukin, M. D. & Imamoglu, A. Quantum measurement of a mesoscopic spin ensemble. *Phys. Rev. A* **74,** 032316 (2006).
12. Manson, N. B., Harrison, J. P. & Sellars, M. J. Nitrogen-vacancy center in diamond: model of the electronic structure and associated dynamics. *Phys. Rev. B* **74,** 104303 (2006).
13. Dutt, M. V. G. *et al.* Quantum register based on individual electronic and nuclear spin qubits in diamond. *Science* **316,** 1312–1316 (2007).
14. Neumann, P. *et al.* Single-shot readout of a single nuclear spin. *Science* **329,** 542–544 (2010).
15. Maze, J. *et al.* Nanoscale magnetic sensing with an individual electronic spin in diamond. *Nature* **455,** 644–647 (2008).
16. Balasubramanian, G. *et al.* Nanoscale imaging magnetometery with diamond spins under ambient conditions. *Nature* **455,** 648–651 (2008).
17. Childress, L., Taylor, J. M., Sørensen, A. S. & Lukin, M. D. Fault-tolerant quantum communication based on solid-state photon emitters. *Phys. Rev. Lett.* **96,** 070504 (2006).
18. Togan, E. *et al.* Quantum entanglement between an optical photon and a solid-state spin qubit. *Nature* **466,** 730–734 (2010).
19. Robledo, L., Bernien, H., van Weperen, I. & Hanson, R. Control and coherence of the optical transition of single nitrogen vacancy centers in diamond. *Phys. Rev. Lett.* **105,** 177403 (2010).
20. Santori, C. *et al.* Coherent population trapping of single spins in diamond under optical excitation. *Phys. Rev. Lett.* **97,** 247401 (2006).
21. Buckley, B. B., Fuchs, G. D., Bassett, L. C. & Awschalom, D. D. Spin-light coherence for single-spin measurement and control in diamond. *Science* **330,** 1212–1215 (2010).
22. Maze, J. R. *et al.* Properties of nitrogen-vacancy centers in diamond: the group theoretic approach. *N. J. Phys.* **13,** 025025 (2011).
23. Fuchs, G. D. *et al.* Excited-state spectroscopy using single spin manipulation in diamond. *Phys. Rev. Lett.* **101,** 117601 (2008).
24. Klauser, D., Coish, W. A. & Loss, D. Nuclear spin state narrowing via gate-controlled Rabi oscillations in a double quantum dot. *Phys. Rev. B* **73,** 205302 (2006).
25. Dolde, F. *et al.* Electric-field sensing using single diamond spins. *Nature Phys.* **7,** 459–463 (2011).
26. Siyushev, P. *et al.* Monolithic diamond optics for single photon detection. *Appl. Phys. Lett.* **97,** 241902 (2010).
27. Chen, G., Bergman, D. L. & Balents, L. Semiclassical dynamics and long-time asymptotics of the central-spin problem in a quantum dot. *Phys. Rev. B* **76,** 045312 (2007).
28. Bardou, F., Bouchaud, J.-P., Aspect, A. & Cohen-Tannoudji, C. *Lévy Statistics and Laser Cooling: How Rare Events Bring Atoms to Rest* (Cambridge Univ. Press, 2002).
29. Rudner, M. S., Vandersypen, L. M. K., Vuletic, V. & Levitov, L. S. Generating entanglement and squeezed states of nuclear spins in quantum dots. Preprint at ⟨http://arxiv.org/abs/1101.3370⟩ (2011).
30. Verstraete, F., Wolf, M. M. & Cirac, J. I. Quantum computation and quantum-state engineering driven by dissipation. *Nature Phys.* **5,** 633–636 (2009).

Supplementary Information is linked to the online version of the paper at www.nature.com/nature.

Acknowledgements We thank A. Aspect, J. I. Cirac, G. Giedke, M. Gullans, J. Hodges, M. Issler, V. Jacques, F. Jelezko, E. Kessler, A. Kubanek, J. McArthur, A. Pick, A. Sipahigil, J. Taylor, S. Yelin and A. S. Zibrov for discussions and experimental help. This work was supported by the NSF, NSF-funded CUA, DARPA (QUEST and QUASAR programmes), ARO MURI, the NDSEG Fellowship, the Packard Foundation and an ERC Advanced Investigator Grant. The content of this paper does not necessarily reflect the position or the policy of the US government, and no official endorsements should be inferred.

Author Contributions All authors contributed extensively to the work presented in this paper.

Author Information Reprints and permissions information is available at www.nature.com/reprints. The authors declare no competing financial interests. Readers are welcome to comment on the online version of this article at www.nature.com/nature. Correspondence and requests for materials should be addressed to M.D.L. (lukin@fas.harvard.edu).